Available online at www.sciencedirect.com
SCIENCE DIRECT®
ELSEVIER
Applied Surface Science 220 (2003) 79–87
applied surface science
www.elsevier.com/locate/apsusc

AFM and SEM characterization of non-toxic vanadium-free Ti alloys used as biomaterials

C. Morant[a,*], M.F. López[b], A. Gutiérrez[a], J.A. Jiménez[c]

[a]*Departamento de Física Aplicada, Universidad Autónoma de Madrid, Cantoblanco, E-28049 Madrid, Spain*
[b]*Instituto de Ciencia de Materiales de Madrid, CSIC, Cantoblanco, E-28049 Madrid, Spain*
[c]*Centro Nacional de Investigaciones Metalúrgicas, CSIC, Avda. Gregorio del Amo 8, E-28040 Madrid, Spain*

Received 1 April 2003; received in revised form 21 May 2003; accepted 21 May 2003

Abstract

In this work, three titanium alloys have been studied by means of atomic force microscopy (AFM) and scanning electron microscopy (SEM) to determine their surface topography. The alloys investigated were Ti–6Al–7Nb, Ti–13Nb–13Zr, and Ti–15Zr–4Nb, with no presence of the toxic element V, and with a possible use as biomaterials for osteoarticular prostheses. These alloys were studied at room temperature and also after a thermal treatment at 750 °C during 24 h, which produces a protective surface oxide layer. The aim of the present work is to compare the surface structure and morphology of the alloys, both as-received and after the oxide layer was formed at elevated temperature.

Keywords: Atomic force microscopy; Scanning electron microscopy; Oxidation; Titanium alloys; Biomaterials

1. Introduction

It is known that Ti alloys are good materials for technological and biomedical applications [1–4]. The most used Ti alloy for implants is Ti–6Al–4V, with excellent mechanical properties. However, the vanadium component has revealed to be a toxic element that provides bad biocompatibility and, consequently, it must be avoided in medical applications like human implants [5]. This work is part of an extensive study aimed to investigate new Ti alloys without vanadium in order to find a good substitute for the most used Ti–6Al–4V alloy [6–9].

In the last years, atomic force microscopy (AFM) has become a useful technique for the study of the surface structure of materials [10–15]. An important application of AFM is high resolution imaging of different biomaterial surfaces with the aim of studying their topography. As it has been previously investigated, there exists an influence of the roughness and topography of a biomaterial on its in vivo and in vitro cytocompatibility [16,17]. Therefore, the complete characterization of a biomaterial must include the investigation of its surface morphology.

In this study, atomic force microscopy (AFM) was applied to characterize the surface of three Ti alloys without V: Ti–6Al–7Nb, Ti–13Nb–13Zr, and Ti–15Zr–4Nb. These three materials have already provided good biocompatibility [6], and their mechanical properties are also satisfactory. For each alloy,

* Corresponding author. Tel.: +34-91-3974924; fax: +34-91-3973969.
E-mail address: c.morant@uam.es (C. Morant).

0169-4332/$ – see front matter © 2003 Elsevier B.V. All rights reserved.
doi:10.1016/S0169-4332(03)00746-3

two surface states were investigated: the as-received state, with a thin, natural passive layer, and a high-temperature oxidized state, where a thicker oxide scale is developed. If the composition and morphology of this scale is appropriate, the biocompatibility of the alloys can be improved. In previous studies, the corrosion behavior as well as the surface composition of both surface states have been investigated [6–9]. After the satisfactory results obtained, a next step to further characterize these Ti alloys can be the study of their surface morphology and topography. Such an investigation is relevant in the case of biomedical applications since the tissular cells will be in direct contact with the alloy topmost surface. Consequently, AFM has been used for the topographic characterization at nanometric scale. In order to extend the study to a microscopic scale, scanning electron microscopy (SEM) was also used to image the same surfaces. The results shown in this work from both microscopies prove the complementarity of these instruments.

The purpose of the present work is to investigate the topography, phase separation and evolution of the surface micro-morphology of these three alloys before and after the high-temperature oxidation process.

2. Experimental

The chemical composition of the three titanium alloys was (in wt.%): Ti–7Nb–6Al, Ti–13Nb–13Zr and Ti–15Zr–4Nb. The corresponding atomic percent composition (at.%) is Ti–10.4Al–3.6Nb, Ti–7.8Zr–7.7Nb and Ti–8.7Zr–1.3Nb, respectively. In the following, the weight percent composition will be used to identify the samples. The alloys were prepared by melting high purity Ti (99.9%) with the corresponding amount of each alloying element, also of high purity. It was used an electric arc furnace under vacuum, and the melt was casted in a cooper coquille. The homogeneity of the alloys was determined with the aid of an optical and a scanning electron microscope (SEM) equipped with energy dispersive X-ray (EDX) microanalysis. The EDX spectra of the different alloys showed neither deviation from the nominal composition nor the presence of impurities. Additionally, the nominal composition was confirmed by performing X-ray photoelectron spectroscopy (XPS) on the as-received specimens after cleaning the surface with Ar ion sputtering. The specimens were cut from as-cast ingots by electrospark-erosion.

Pure titanium presents at room temperature a hexagonal close-packed (hcp) crystal structure, which is referred to as α-phase. This structure transforms to a body-centered cubic (bcc) crystal structure, which is called β-phase, at 883 °C, as confirmed by X-ray diffraction. This transformation temperature from α- to β-phase can be raised or lowered by adding alloying elements. The elements that when dissolved in titanium raise the transformation temperature stabilize the α-phase, and those decreasing this temperature are β-stabilizers. From the alloying elements present in the alloys studied, Al is an α-stabilizing element, Zr is regarded as a neutral element and Nb stabilizes the β-phase. As observed in the equilibrium phase diagrams of numerous titanium-base alloys, the α- and β-regions are separated by a two phase region α + β region [18]. Thus, an annealing procedure was followed in all samples with the aim of obtaining a two phase (α + β) microstructure, which ensures satisfactory mechanical properties. Thus, the alloys were annealed above the β-transition temperature at 1100 °C for 1 h and aged at 700 °C for 1 h. Afterwards, samples were taken out of the furnace to cool down. The samples were abraded and polished using diamond pastes with successively finer particle size. In the final stage of this process, colloidal silica was used to ensure a surface free of mechanical deformation. Finally, the samples were ultrasonically cleaned in acetone. The material in this state was labeled as the ''as-received'' sample. At this time, different samples were isothermally oxidized at 750 °C in air for 24 h.

The micro- and nano-structure of the three Ti alloys were determined using a SEM equipped with EDX and an atomic force microscope (AFM). The EDX spectra allowed to evaluate the distribution of alloying elements in the two phases present in the alloys. Thus, the estimation of the concentration of α or β stabilizers was used for the determination of the alloys microstructure. A metallographic preparation of the samples was required for SEM analysis, including mounting the samples in bakelite and polishing by the conventional method. AFM measurements did not require additional sample preparation and were performed under ambient conditions with a commercial microscope [19] using rectangular Si_3N_4 cantilevers (NT-MTD, Russia, nominal spring constant of 0.6 N/m).

The AFM images were mainly obtained in contact mode, applying a maximum normal force of a few nanoNewton. Images were recorded at typical rates of 1.0 s per scan line. The scan rate was changed from 1.0 to 2.0 s per scan line depending on the roughness of the surface and the scanned area, i.e. slower images for rougher surfaces and for bigger area scanned. Some images were also obtained in jumping mode [20].

3. Results and discussion

Representative AFM images of the three as-received Ti alloys surfaces are shown in Fig. 1. For the as-received Ti–6Al–7Nb alloy, it is possible to distinguish a lamellar structure caused by the different phases that are present. In these lamellar areas, granular structures can be observed in a magnified image taken with a better resolution (3 μm × 3 μm). The morphology of the as-received Ti–13Nb–13Zr alloy, represented in Fig. 1b, shows clearly the lamellar (α + β) microstructure. This result agrees with previous SEM images obtained for this alloy in the as-received condition [6]. The surface of this sample, as it is observed by SEM [6] and AFM (Fig. 1b), is completely covered by a lamellar structure. This effect did not occur with the as-received Ti–6Al–7Nb sample (Fig. 1a). This result is coherent with the EDX analysis

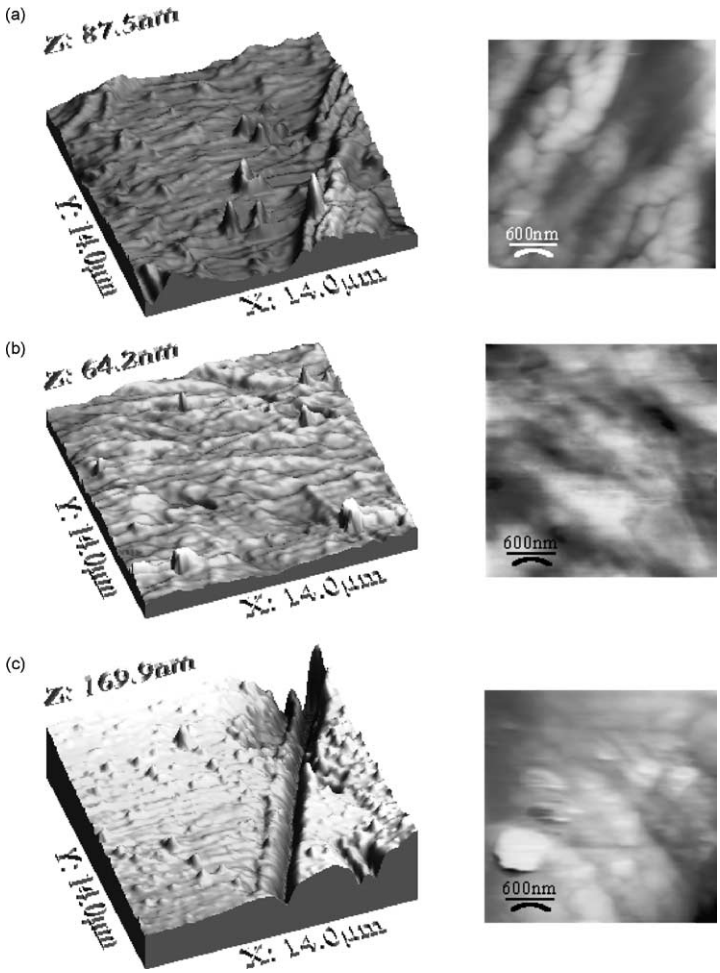

Fig. 1. AFM topographic images (14 μm × 14 μm (left images) and 3 μm × 3 μm (right images)) of as received alloys: (a) Ti–6Al–7Nb; (b)Ti–13Nb–13Zr; (c)Ti–15Zr–4Nb.

performed previously [6] that showed a similar distribution of both phases for the case of Ti–13Nb–13Zr, while Ti–6Al–7Nb presented predominantly α-phase. Finally, in the AFM image of the as-received Ti–15Zr–4Nb alloy showed in Fig. 1c, it can be clearly distinguished a longitudinal groove on the surface of the material. This kind of grooves was observed across all the imaged surface area and will be commented below.

One of the advantages of the AFM is the ability of acquiring simultaneously topographic and lateral (i.e. friction) images [21,22]. The frictional forces between the AFM probe and sample surface lead to torsion of the AFM cantilever around its horizontal axis. This torsion is reflected in the lateral AFM images, where different frictional forces appear bright and dark. It should be pointed out that the normal displacement of the lever contributes to the lateral force. Then, the friction measurements could be locally modified by the sample topography [23], especially in rough samples and when the morphology is not homogeneous. But even if it is difficult to make reliable absolute measurements of friction by means of the AFM, it is always possible to make a comparative study of the friction behavior for the different alloys. Differences in the chemical surface composition may cause a different frictional interaction between the tip and the surface structure as long as each composition has a different friction coefficient. Thus, these differences could be recorded and transferred into AFM images. As an example, Figs. 2a and b represent the simultaneous topographic and frictional AFM images of the as-received Ti–13Nb–13Zr alloy surface, respectively. Different intensities (dark and light colors) can be observed for the lamellar structures in both images. There is not an evident correlation between the intensities of the topographic image and those of the friction image. This clearly indicates that the different structures show different friction behavior. Although in the AFM topographic images the observed structure cannot be associated with different phases, the simultaneous lateral imaging showed evidence of areas with different friction values that can be associated with the α- and β-phases already analyzed by SEM–EDX [6]. One has to note that the interaction between the microscope tip and the samples occurs at the outermost surface. The presence of the passive layer involves the presence of oxides at the surface, which cannot be identified directly as Ti α- or β-phase, although they originated from bulk α- and β-phases. A different friction may result from a different polar character of the passive layer regions associated to the bulk phase, leading to different interaction between the Si_3N_4 probe and the surface. We conclude that the frictional contrast correlates with the lateral structure of dark and bright lamellar phases and confirms the microstructure obtained by SEM–EDX.

A thermal treatment was performed with the aim of generating a protective oxide layer on the alloy surfaces. The task of this oxide layer is the improvement of the corrosion resistance of the material and, therefore, its biocompatibility. In previous works, the

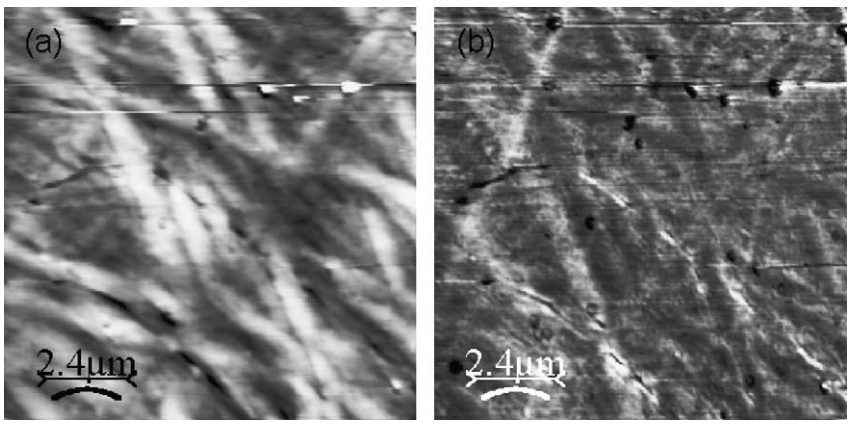

Fig. 2. AFM images (12 μm × 12 μm) of as received Ti–13Nb–13Zr alloy: (a) topographic image and (b) corresponding lateral force (friction) image.

corrosion behavior of these oxidized alloys as well as the chemical analysis of the oxide layers was determined [7–9]. According to these results, the oxidized layers are composed mainly of TiO_2 for Ti–13Nb–13Zr and Ti–15Zr–4Nb alloys and of Al_2O_3 for Ti–6Al–7Nb. Both the oxides, TiO_2 and Al_2O_3, are widely known for their good biocompatibility. However, the determination of the morphology of the surface is also essential for a complete characterization as a biomaterial. Top views of the surfaces of the Ti–6Al–7Nb, Ti–13Nb–13Zr and Ti–15Zr–4Nb alloys oxidized for 24 h at 750° are shown in Figs. 3 and 4, using AFM and SEM, respectively. From the AFM images, several parameters can be extracted to obtain essential information on the surface topography. Thus, the root mean square (RMS) roughness and mean grain size obtained after the analysis of different AFM images, both before and after oxidation, are presented in Table 1. The values of the grain size correspond to the mean diameter of the features observed on at least four representative AFM images (3000 nm × 3000 nm). These values were established measuring several

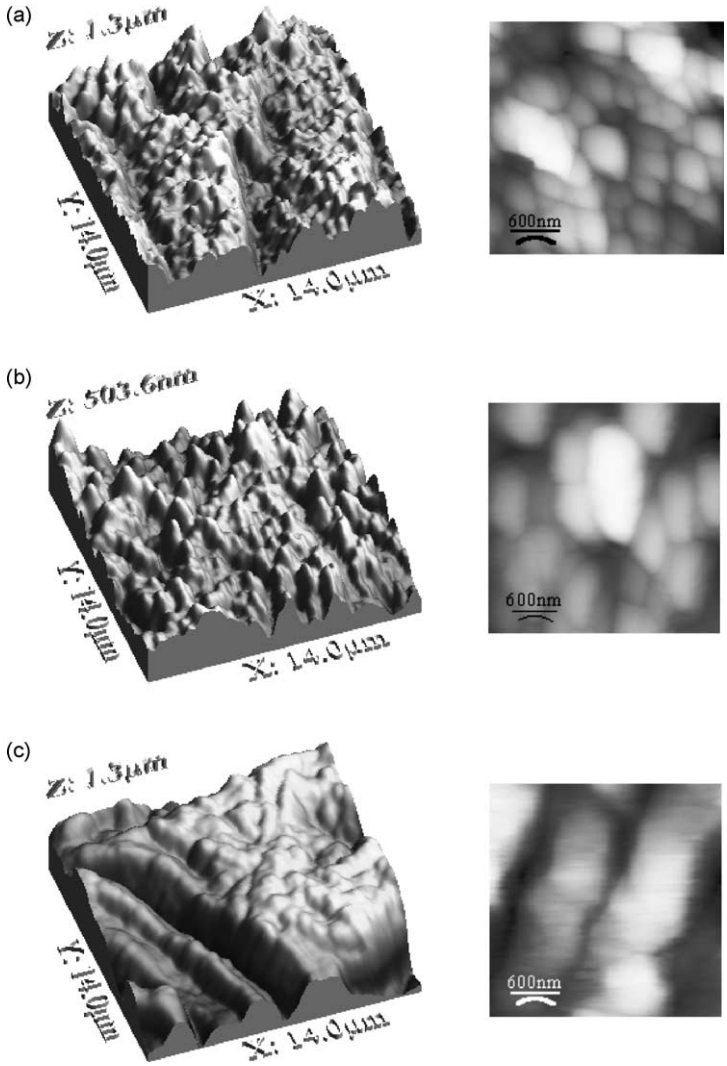

Fig. 3. AFM topographic images (14 μm × 14 μm (left images) and 3 μm × 3 μm (right images)) of oxidized alloys for 24 h at 750 °C: (a) Ti–6Al–7Nb; (b)Ti–13Nb–13Zr; (c)Ti–15Zr–4Nb.

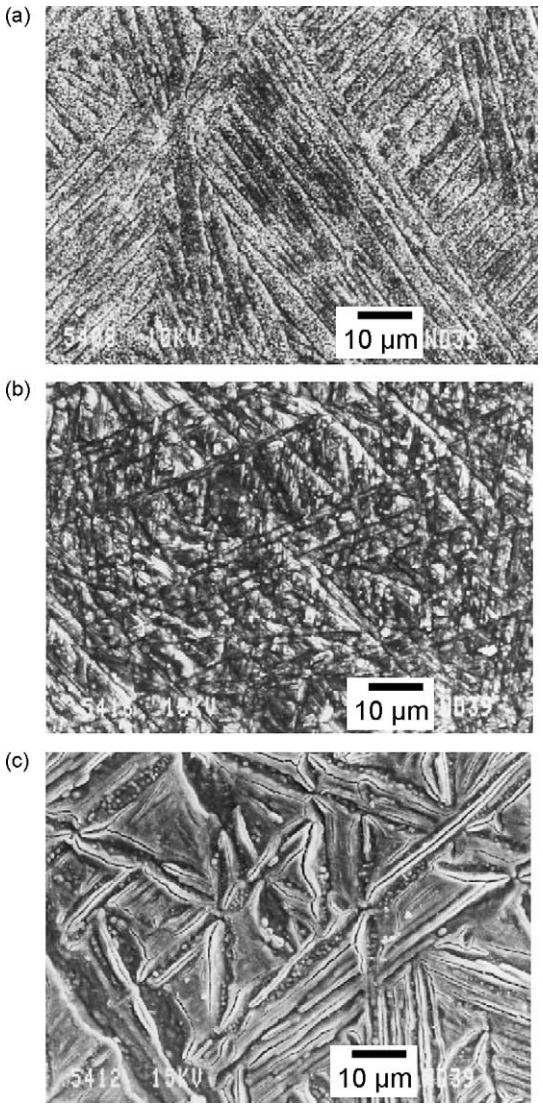

Fig. 4. SEM micrographs of: (a) Ti–6Al–7Nb; (b)Ti–13Nb–13Zr; (c)Ti–15Zr–4Nb, after an oxidation treatment at 750 °C for 24 h.

profiles along the surface images. The roughness was given by the root mean square value (RMS) of the topographic data [19]. The RMS surface roughness from different materials obtained with AFM can only be compared with images acquired in similar area size scanned. The RMS values presented in Table 1 correspond to the larger AFM measured area, 14 μm × 14 μm, conforming the more regular obtained surfaces.

Analyzing the data from Table 1, it can be observed that the morphology of all the as-received samples

Table 1
Root mean square (RMS) roughness and mean size grain parameters from AFM images

Alloy	Oxidation time (h)	RMS roughness σ (nm)	Mean size grain diameter (nm)
Ti–6Al–7Nb	0	10.8 ± 3.7	275 ± 47
Ti–13Nb–13Zr	0	2.8 ± 0.8	230 ± 88
Ti–15Zr–4Nb	0	25.2 ± 8.3	259 ± 90
Ti–6Al–7Nb	24	210.1 ± 50	399 ± 109
Ti–13Nb–13Zr	24	124.0 ± 20	609 ± 144
Ti–15Zr–4Nb	24	223.1 ± 74	1020 ± 227

presents low RMS roughness values and the structures on the surface have a similar diameter size. However, the oxidation process leads to a large increase of both the surface roughness and the grain size. In the case of roughness, the increase is between one and two orders of magnitude (a factor of ∼20 for the Ti–6Al–7Nb sample, a factor of ∼50 for the Ti–13Nb–13Zr sample, and a factor of ∼10 for the Ti–15Zr–4Nb sample). This huge increase and the large differences between samples indicate that the final roughness is governed by the oxidation process and kinetics. On the other hand, the increase in mean grain size is more moderate, suggesting that some of the alloy morphology is transmitted to the oxide surface. The lowest difference between oxide and alloy surface corresponds to the Ti–6Al–7Nb. This sample is the one with better correlation between non-oxidized and oxidized surface morphology.

It is very important to notice that the RMS roughness for the Ti–15Zr–4Nb sample oxidized for 24 h was higher than the Ti–7Nb–6Al alloy oxidized for 24 h in the case of large scanned surface areas (>10 μm × 10 μm). However, for intermediate scanned areas (5 μm × 5 μm) similar RMS values were found in both samples. A comparison of these roughness values with the morphology presented in SEM images (Fig. 4) can be made for large imaged scales. It can be detected that the surface of the Ti–15Zr–4Nb alloy oxidized for 24 h is very abrupt, while that of the Ti–7Nb–6Al alloy oxidized for 24 h is more homogeneous at every scale. Considering the potential applications of the alloys as biomaterials, the most appropriate surface should be homogeneous and with large roughness values in order to promote a perfect adherence for tissular cells. From this point of view, the oxidized Ti–6Al–7Nb sample seems to be the one with best properties.

The surface morphology at nano- and microscopic scale of the different alloys after the oxidation process can be extracted from representative AFM and SEM images showed in Figs. 3 and 4. For the Ti–7Nb–6Al alloy, the surface roughness increases abruptly after 24 h of oxidation. An interesting point is the granular structure observed on the surface, that provides a regular topography (Fig. 3a). The same surface was imaged with SEM (Fig. 4a) and it was possible to detect nanometric circular forms in concordance with the morphology observed by AFM. This granular structure is embedded in a corrugated superstructure at a micrometric scale, as observed in the SEM image. Some of the grooves can also be observed in the AFM images of Fig. 3a. In the SEM image of Fig. 4a, several regions of this superstructure with different directions of the grooves can be observed separated by well-defined b orders between regions. This suggests that the wrinkled microstructure originates from the alloy microcrystalline structure, corresponding the different groove directions to different crystalline orientations.

The mean dimension obtained by AFM for the corrugated terraces is 3.3 μm wide, with a step between terraces of 350 nm. As can be observed in Figs. 3a and 4a, the dimensions of the SEM bands and AFM terraces are in concordance.

The Ti–13Nb–13Zr alloy after 24 h of oxidation also shows the presence of circular structures of submicrometric size (Figs. 3b and 4b). These structures have a larger size than those observed for Ti–7Nb–6Al oxidized for 24 h (Fig. 3a and b), and no superstructure at micrometric scale is observed. Moreover, its RMS surface roughness did not increase as much as that of the Ti–7Nb–6Al oxidized sample (see Table 1).

For the case of the Ti–15Zr–4Nb alloy, as it has been commented earlier, the RMS roughness and mean grain size (Table 1) have higher values after oxidation than the other described alloys. In the AFM image of the oxidized sample, deep longitudinal grooves across all the surface area can be observed. The depth of these grooves had a mean value of 350 nm. These grooves are the cause of the high RMS roughness values obtained. It is worthy noting that a similar RMS increase with oxidation was achieved in the Ti–7Nb–6Al alloy oxidized for 24 h, but in that case the increase is more uniform. For the Ti–15Zr–4Nb oxidized alloy, the RMS increase was almost exclusively originated by the surface fissures.

We have also performed AFM measurements working in jumping mode. This new measurement mode can collect simultaneously the topographic image and an additional physical property of the sample. The jumping mode consists essentially in the following procedure: at each image point first the topography of the sample is measured and, then, at the same point, a force versus Z displacement curve is achieved. Then, the tip is brought to the next image point out of contact with the sample. A detailed explanation of the working principle of the AFM in jumping mode is given in [20]. Since the lateral motion is done out of contact, this method is nearly free of shear forces and a much better resolution can be obtained in the topography images. In order to compare the topographic data, first of all we imaged an area of 3 μm × 3 μm for the Ti–7Nb–6Al alloy in contact mode and consecutively the same area in jumping mode. In this way, we could check the validity of this new AFM measurement mode: the morphology and RMS values were the same in topographic images of both modes. Afterwards, a larger area (12 μm × 12 μm) was acquired in jumping mode. The high resolution of this topographic image, presented in Fig. 5, shows a clear columnar growth of the oxides on the surface. This kind of growth is the reason of the high RMS roughness values and the homogeneous distribution of circular structures on big terraces observed in Figs. 3a and 4a.

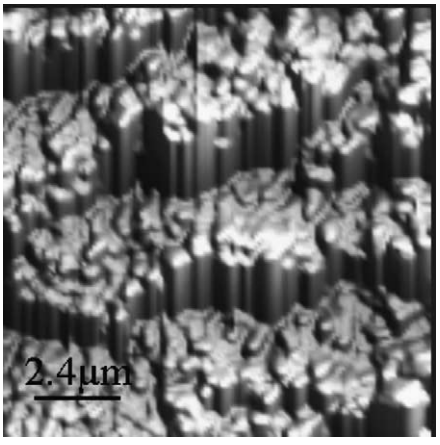

Fig. 5. Topographic AFM image (12 μm × 12 μm) of Ti–7Nb–6Al obtained in jumping mode and showing a clear columnar growth after an oxidation treatment at 750 °C for 24 h.

4. Conclusions

The surface structure and the topography of the three titanium alloys developed for biomedical applications were investigated by AFM and SEM. These alloys were studied in the as-received state and also after a thermal treatment. In the as-received state, the material is protected by the passive layer generated spontaneously on the surface by air contact of the alloy. The aim of the thermal treatment process is to develop a thicker oxide layer on the material surface, which could enhance the corrosion resistance of the alloy.

For the as-received samples, the AFM images are in accordance with previous SEM investigations showing for the Ti–7Nb–6Al the presence of one phase (α-phase) and for Ti–13Nb–13Zr the presence of two phases (α- and β-phases). The frictional images confirm, for the Ti–13Nb–13Zr sample, the presence of two different phases, which constitute the microstructure of the alloy. For the case of the Ti–15Zr–4Nb alloy, the AFM exhibits the presence of several longitudinal grooves.

Concerning the 24 h oxidized alloys, Ti–7Nb–6Al shows a granular structure on big terraces with a rather regular topography. The Ti–13Nb–13Zr oxidized alloy exhibits also circular structures but the presence of terraces is not observed. Finally, the Ti–15Zr–4Nb oxidized alloy shows deep longitudinal grooves across all scanned surface area.

The AFM measurements performed in jumping mode provide information about the origin of the terraces observed for the oxidized Ti–7Nb–6Al alloy. Since this mode gives a much better resolution, a clear columnar growth of the oxides on the surface could be detected.

In summary, it has been observed that the oxidized layer formed on the Ti–7Nb–6Al alloy after 24 h of thermal treatment shows the absence of longitudinal grooves and a regular topography. Taking into account from previous works that this oxidized layer is compact and uniform providing a satisfactory corrosion behavior, it is possible to predict its suitability for biomedical applications.

Acknowledgements

The authors are gratefully acknowledged to Prof. G. Fommeyer from Max Planck Institut für Eisenforschung (Düsseldorf) for kindly supplying the Ti alloys specimens. This work has been supported by the Project 07N-0050-1999 of the Spanish ''Programa de Tecnología de los Materiales de la Comunidad Autónoma de Madrid'' and the Project MAT99-0201 from CICYT of Spain. One of the authors (A. Gutiérrez) thanks the Spanish Ministerio de Ciencia y Tecnología for financial support through the ''Ramón y Cajal'' Programme.

References

[1] H.J. Breme, V. Biehl, J.A. Helsen, Metals and implants, in: J.A. Helsen, H.J. Breme (Eds.), Metals as Biomaterials, Wiley, Chichester, 1998, pp. 37–72.
[2] R. Boyer, G. Welsch, E.E. Collings, Titanium alloys, Materials Properties Handbook, Materials Park, ASM International, Ohio, 1994.
[3] H. Sibum, V. Güther, O. Roidl, Titanium, in: F. Habashi (Ed.), Alloys, Wiley–VCH, Weinheim, 1998, pp. 213–219.
[4] D.H. Kohn, P. Ducheyne, Materials for bone and joint replacement, in: D.F. Williams (Ed.), Medical and Dental Materials, Series Materials Science and Technology, vol. 14, VCH, Weinheim, 1992, pp. 31–56.
[5] Y. Okazaki, S. Rao, Y. Ito, T. Tateishi, Corrosion resistance, mechanical properties, corrosion fatigue strength and cytocompatibility of new Ti alloys without Al and V, Biomaterials 19 (1998) 1197–1215.
[6] M.F. López, A. Gutiérrez, J.A. Jiménez, In vitro corrosion behavior of Ti alloys without V for biomedical applications, Electrochim. Acta 47 (2002) 1359–1364.
[7] M.F. Lopez, A. Gutiérrez, J.A. Jiménez, Surface characterization of new non-toxic titanium alloys for use as biomaterials, Surf. Sci. 482–485 (2001) 300–305.
[8] M.F. López, L. Soriano, F.J. Palomares, M. Sánchez-Agudo, G.G. Fuentes, A. Gutiérrez, J.A. Jiménez, Soft X-ray absorption spectroscopy study of passive and oxide layers of titanium alloys, Surf. Interface Anal. 33 (2002) 570–576.
[9] M.F. López, J.A. Jiménez, A. Gutiérrez, Corrosion study of oxidized titanium alloys, Electrochim. Acta 48 (2003) 1395–1401.
[10] K.D. Jandt, Atomic force microscopy of biomaterials surfaces and interfaces, Surf. Sci. 491 (2001) 303–332.
[11] C.A. Siedlecki, R.E. Marchant, Atomic force microscopy for characterization of the biomaterial interface, Biomaterials 19 (1998) 441–454.
[12] A.M. Ektessabi, H. Kimura, Characterization of the surface of bio-ceramic thin films, Thin Solid Films 270 (1995) 335–340.
[13] K.D. Jandt, M. Finke, P. Cacciafesta, Aspects of the physical chemistry of polymers, Colloid Surf. Part B 19 (2000) 301–314.
[14] X.P. Luo, N. Silikas, M. Allaf, N.H.F. Wilson, D.C. Watts, AFM and SEM study of the effects of etching

on IPS-Empress 2™ dental ceramic, Surf. Sci. 491 (2001) 388–394.
[15] I.B. Leonor, A. Ito, K. Onuma, N. Kanzaki, R.L. Reis, In vitro bioactivity of starch thermoplastic–hydroxyapatite composite biomaterials: an in situ study using atomic force microscopy, Biomaterials 24 (2003) 579–585.
[16] K. Anselme, P. Linez, M. Bigerelle, D. Le Maguer, A. Le Maguer, P. Hardouin, H.F. Hildebrand, A. Iost, J.M. Leroy, The relative influence of the topography and chemistry of $TiAl_6V_4$ surfaces on osteoblastic cell behavior, Biomaterials 21 (2000) 1567–1577.
[17] P. Cacciafesta, K.R. Hallam, A.C. Watkinson, G.C. Allen, M.J. Miles, K.D. Jandt, Visualisation of human plasma fibrinogen adsorbed on titanium implant surfaces with different roughness, Surf. Sci. 491 (2001) 405–420.
[18] R. Boyer, Metallography and microstructures, Metals Handbook, vol. 9, Materials Park, ASM International, Ohio, 1985.
[19] Nanotec Electronica (http://www.nanotec.es).
[20] P.J. De Pablo, J. Colchero, J. Gómez-Herrero, A.M. Baró, Jumping mode scanning force microscopy, Appl. Phys. Lett. 73 (1998) 3300–3302.
[21] C.M. Mate, G.M. McClelland, R. Erlandsson, S. Chiang, Atomic-scale friction of a tungsten tip on a graphite surface, Phys. Rev. Lett. 59 (1987) 1942–1945.
[22] O. Marti, J. Colchero, J. Mlynek, Combined scanning force and friction microscopy of mica, Nanotechnology 1 (1990) 141–144.
[23] D.F. Ogletree, R.W. Carpick, M. Salmeron, Calibration of frictional forces in atomic force microscopy, Rev. Sci. Instrum. 67 (1996) 3298–3306.